

# Recent Advances in Moving-Source Beamforming

Svend Gade, Jørgen Hald, Jesper Gomes, Gijs Dirks and Bernard Ginn  
Brüel & Kjær Sound & Vibration Measurements, Nærum, Denmark

A measurement technique is described for the localization and visualization of noise sources on moving sources using beamforming. Delay-and-sum (DAS) beamforming is often used on stationary (fixed) sources. However, the method can also be applied to moving sources such as road vehicles, rail vehicles, aircraft flyovers and rotating blades on wind turbines. Recently, shading techniques have been introduced to compensate for the varying density of microphones and for air turbulence, which will be present for outdoor measurements. This article describes a commercially available system, which includes DAS beamforming and shading techniques dedicated to moving sound sources.

The increased complexity of today's exterior vehicle noise test procedures along with requirements for accuracy and full documentation of the measurement chain have added to the test burden for vehicle manufacturers and their suppliers. Many engineers and technicians who perform pass-by noise measurements also want to perform troubleshooting of the various noise source contributions at the same time. The beamforming option, road vehicle moving-source beamforming (MSB) is an efficient method to yield noise maps and sound power contribution spectra from moving cars or trucks. It also provides the ISO sound pressure level taken from the array to compare with that obtained from pass-by conformance testing.

Beamforming<sup>1,2</sup> is an array-based measurement technique for sound source localization at medium to long distances. Basically, source localization is performed by estimating the amplitudes of plane (or spherical) waves incident toward the array from a chosen set of directions. The angular resolution is inversely proportional to the array diameter measured in units of wavelength, so the array should be much larger than the wavelength to obtain a fine angular resolution. At low frequencies, this requirement usually cannot be met, so the angular resolution will be poor.

For typical, irregular array designs, the beamforming method does not allow the measurement distance to be much smaller than the array diameter. On the other hand, the measurement distance should be kept as small as possible to achieve the finest possible resolution on the source surface. This is not possible when measuring large objects, because the calculation area is limited by the angular coverage.

The use of a discrete set of measurement points on a plane can be seen as a spatial sampling of the sound field. Near-field acoustical holography (NAH) as well as statistically optimized (SONAH) require a grid spacing less than half a wavelength at the highest frequency of interest.<sup>3</sup> On the other hand, beamforming can be applied with array geometries having more than a half wavelength element spacing. For a regular grid array, however, the effect will be strong spatial aliasing, showing up as an ambiguity in the source direction estimation. Use of optimized, irregular arrays can reduce the spatial aliasing effects to an acceptable level up to a much higher frequency with the same average spatial sampling density. This indicates why beamforming can measure up to high frequencies and provide good resolution with a fairly low number of microphones.

Beamforming is an attractive alternative and supplement to NAH/SONAH, because measurements can be taken at some intermediate distance from the source with a highly sparse array. Furthermore, at high frequencies, beamforming can provide quite good resolution. The combined use of beamforming and SONAH covers a wide frequency range.<sup>3</sup>

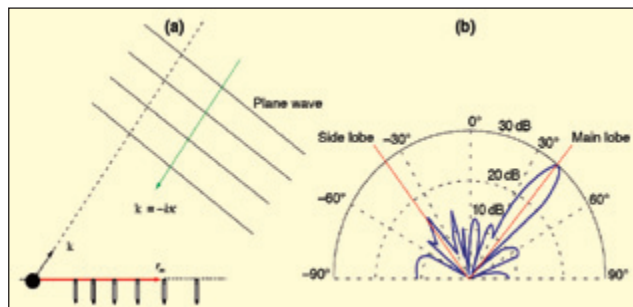


Figure 1. (a) A microphone array, far-field focus direction, and plane-wave incident from the focus direction; (b) Directional sensitivity diagram with main lobe in the focus direction and lower side lobes in other directions.

## Theory of Beamforming

As illustrated in Figure 1, we consider a planar array of  $M$  microphones at  $M$  distributed locations  $r_m$  ( $m=1,2,\dots,M$ ) in the  $xy$  plane of our coordinate system. When such an array is applied for far-field DAS beamforming, the measured pressure signals  $p_m$  are individually delayed and then summed:<sup>(2)</sup>

$$b(\kappa, t) = \sum_{m=1}^M p_m(t - \Delta_m(\kappa)) \quad (1)$$

The individual time delays  $\Delta_m$  are chosen with the aim of achieving selective directional sensitivity in a specific direction, characterized here by a unit vector  $\kappa$ . This objective is met by adjusting the time delays in such a way that signals associated with a plane wave, incident from the direction  $\kappa$ , will be aligned in time before they are summed. Geometrical considerations (see Figure. 1) show that this can be obtained by choosing:

$$\Delta_m = \frac{\kappa \cdot \mathbf{r}_m}{c} \quad (2)$$

where  $c$  is the propagation speed of sound. Signals arriving from other far-field directions will not be aligned before the summation, so they will not coherently add up.

Equation 1 can also be expressed in the frequency domain using auto- and cross-spectra formulations.<sup>2</sup> This is useful when analysing stationary signals.

The width of the main lobe of the array pattern can be estimated from the similarity of the frequency domain version of Eq. 1 with a 2D DFT (Direct Fourier Transform) of a "rectangular" spatial window function covering the area of the array. That is, the main lobe width will be inversely proportional to the diameter  $D$  of the array, and the first "null" will be approximately at  $|K| = K_{\min} = 2\pi/D$ . This main lobe width can be shown to define an on-axis angular resolution equal to  $\lambda/D$ , where  $\lambda$  is the wavelength. At a measurement distance equal to  $L$ , this angular resolution corresponds to a spatial resolution  $R$  given by the expression  $R \approx (L/D)\lambda$ .

The measurement distance  $L$  should not be much smaller than the array diameter  $D$ , so resolution is limited to around one wavelength. For comparison, holography provides a resolution around  $\lambda/2$  at high frequencies and approximately equal to the measurement distance  $L$  at lower frequencies. At low frequencies, therefore, NAH/SONAH can provide significantly better resolution, when a sufficiently small measurement distance is used.

## Beamforming Using Shading

Several options can be applied to minimize any beam-

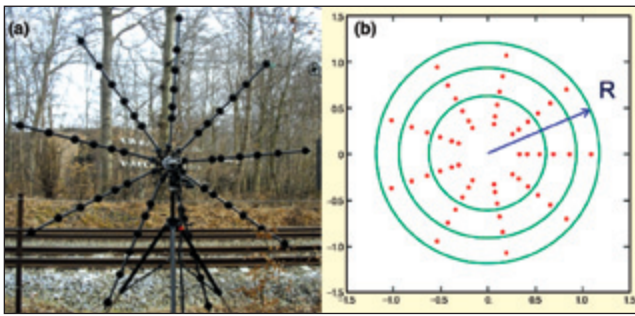


Figure 2. (a) Array example with nine arms and 54 microphones; (b) Area used for zero, some and much turbulence.

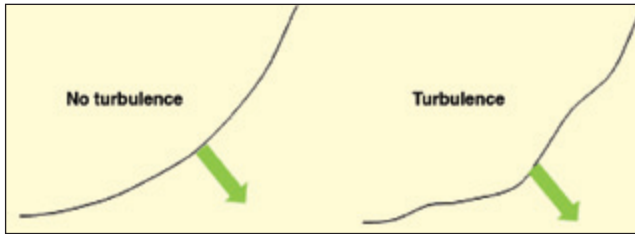


Figure 3. Front of sound wave without and with turbulence.

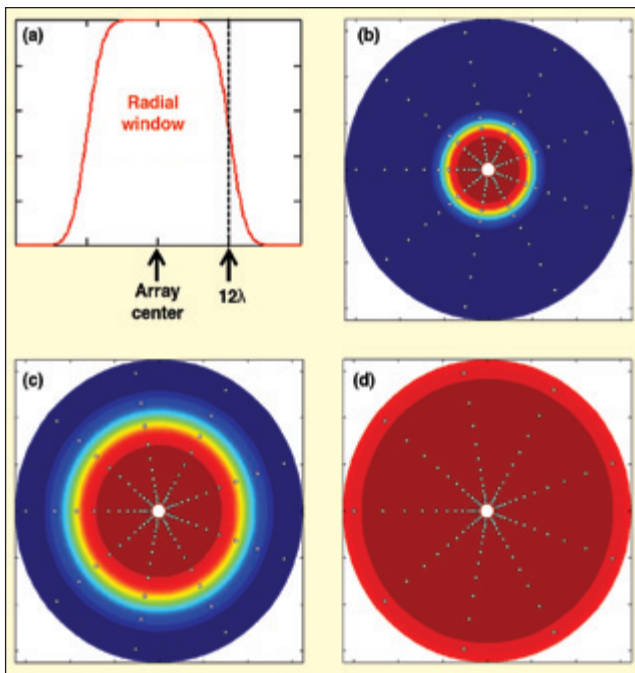


Figure 4. (a) Central subarray weighting function; (b) Central subarray at 2 kHz; (c) Central subarray at 1 kHz; (d) Central subarray at 500 Hz.

forming artefacts or to generally improve the results obtained by standard DAS beamforming. For example by using iterative deconvolution techniques, it is possible to achieve higher resolution than normally provided by DAS beamforming.<sup>4-10</sup> Deconvolution is implemented in the frequency domain on averaged cross-spectra formulation using uncorrelated point-source modelling. Therefore, it cannot easily be applied to a highly nonstationary event such as an accelerated road vehicle pass-by test that typically usually lasts less than two seconds. So the requirement for maps of very short time intervals leaves little or no time for the required averaging.

For outdoor measurements using large arrays, the use of shading should be used to obtain more accurate beamforming results. Outdoor, we will always find turbulence due to wind, local solar heating and vehicles passing by (especially for large vehicles and short measurements). This reduces the signal coherence across the array. Array shading allows for loss of coherence over the array by using a turbulent-dependent subset of microphones (see Figure 2b). With no turbulence, the full array is used; for more turbulence,

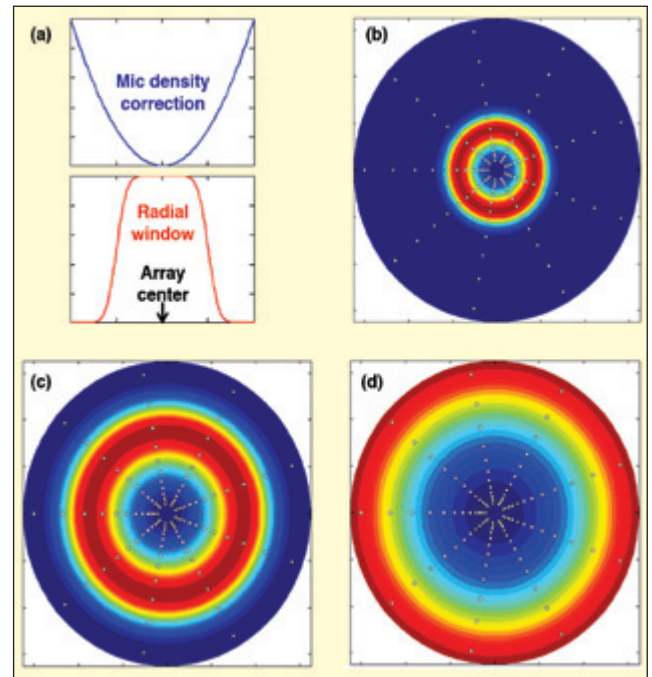


Figure 5. (a) Microphone density correction and radial window; (b) Shading at 2 kHz; (c) Shading at 1 kHz; (d) Shading at 500 Hz.

smaller parts will be used.

To explain the need for using a frequency-dependent shading/weighting function across the array area, we will look at the effect of air turbulence. The main effect of air turbulence is distortion of the wave fronts arriving at the array (see Figure 3).

This distortion has the effect of adding phase modulation to the microphone signals with an amplitude that increases with increasing frequency. For closely spaced microphones, the modulation will be almost equal (within the turbulence structure size) and have no effect on array focusing. For wider microphone separations, the modulation will become more and more incoherent, reducing the coherence between measured microphone signals. Effectively the coherence between two microphone signals will decrease with increasing microphone separation and with increasing frequency.

It can be shown that coherence is retained approximately within a circle of radius  $4000 \text{ m/frequency (Hz)}$  corresponding to a radius of  $12\lambda$ .<sup>8</sup> So at 4 kHz, there will be acceptable coherence only within a radius 1 meter. Instead of using a sharp cut-off and neglecting peripheral microphones, it is recommended to use a frequency-dependent smooth shading/weighting function across the array surface (see Figure 4a). Effectively, only a central subarray of a radius equal to the coherence radius is used.

If we use no shading, the effect of turbulence on DAS beamforming would be an unknown level of reduced resolution, some underestimation and increased noise floor. So, for a single point source, we would not know the response. This is serious in connection with deconvolution, where we have to use a calculated point source response – the so-called Point Spread Function.<sup>7,9,10</sup> Use of shading strongly reduces these unknown effects.

Figure 4a shows an example of a radial cut-off function along a cross section of the array area. The array center and the cut-off position at  $4000 \text{ m/frequency (Hz)}$  equal to approximately 12 wavelengths are indicated. Using shading the effective diameter used in the calculation is now proportional to the wavelength,  $D_{\text{eff}} \approx 24\lambda$ . So in the frequency range, where only a subset of the array is used, an approximate wavelength or frequency-independent angular resolution will be obtained. For a 12-meter diameter array, for example, this will be the case above approximately 700 Hz.

The three contour maps in Figure 4 show the radial window function at three frequencies, superimposed on a 12-m diameter array geometry: 500 Hz, 1 kHz and 2 kHz. At 500 Hz, the cut-off point is outside the array radius, so the cut-off function is almost constant over the entire array area. However, if we use shading functions of the form shown here at 500 Hz, then due to the high

concentration of microphones at the array center, the array will appear as being acoustically small and provide poor resolution.

In addition to radial weighting, array shading is necessary to compensate for the microphone density of the array shown in Figure 2 in order to improve spatial resolution of the calculations. It is obvious that the microphone density is much higher close to the center of the array than close to its periphery.

To compensate for high central microphone density, we multiply by a radial function inversely proportional to microphone density, as shown in Figure 5a. Effectively, the shading function assumes a doughnut shape (Figures 5b-5d). At 500 Hz, the highest weighting will be on the outermost microphones, and the weighting will decrease toward the center, but in such a way that the effective weighting per unit area will be constant. Slightly different variations of shading can be used to obtain either maximum resolution or maximum smoothing results.

## Instrumentation

A road vehicle MSB setup requires a full wheel (often used under free-field conditions) or a half wheel (often used with mirror-ground conditions over a reflecting plane) microphone array, as shown in Figures 2a, 6 and 8. A relatively large diameter of 4 meters or larger is required. The number of microphones is typically between 40 and 100. Then there is need for a measurement front end, a PC and appropriate measurement and beamforming software.

Road vehicle MSB operates as described previously, with the addition of tracking the moving target. In other words, rather than focusing on a point, the array is tracking the moving vehicle by continuously adjusting the time delays. The test area is set up on a straight stretch of road (see Figure 6). The data acquisition functions are set up according to the relationship between the global coordinates (the test area) and the local coordinates (the vehicle). The calculated data are then expressed in terms of the local coordinate system, or the vehicle. In addition to the array shown in Figure 6, also some photocells and a radar are shown.

Road vehicle MSB offers several methods to detect position and speed:

- Position trigger and speed pulses – for variable speed detection using photocells, radar or GPS (used for an accelerating vehicle, for example).
- Position trigger and manually set speed – for fixed speed detection, using a single photocell and finally.
- Dual-position triggers – for fixed speed detection using two photocells.

Road vehicle MSB can also be integrated into and combined with an ISO 362 pass-by system. Doppler effects must also be taken into account. The vehicle moving toward, past and away from the array setup creates a Doppler effect (see Figure 7). It is well known that when the vehicle is approaching the array, the recorded sound is shifted to higher frequencies, and when the vehicle is moving away, the recorded sound is shifted to lower frequencies.

Both for fixed speed as well as accelerating vehicles, for each focus point there is an automatic and continuous Doppler correction. So in maps, the sources will appear with the correct frequency rather than the measured frequency.

Finally, after recording time histories in all measurement channels, up-sampling is utilized to reduce errors rather than unnecessarily devouring massive amounts of data storage space. For example, measurements recorded with 8192 samples/s (as for a typical 3.2 kHz frequency range) are up-sampled by a factor of 16. This method produces less than 10% phase error at 3 kHz (or <0.1 dB error). Not only does up-sampling save storage space, but it also simplifies setup and incurs negligible error.

Calculation intervals are user definable. For pass-by measurements, the calculation intervals are typically made for every 25 cm position interval. So beamforming results are stored as a function of position for each calculation point in the sound map.

## Road Vehicle Measurement Example

Road vehicle MSB measurements were performed on the truck shown in Figure 8 at a speed of about 20 km/h. A 4-channel, half-wheel, planar microphone array at a distance of 7.5 meters



Figure 6. Typical setup for road vehicle moving-source beamforming – array, photocells and radar.

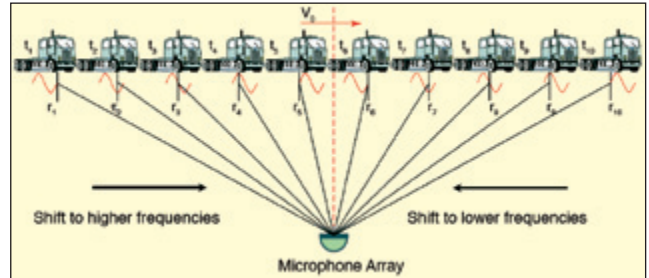


Figure 7. Doppler-effect correction needed for frequency shift.



Figure 8. Truck and half wheel array on test track for road vehicle moving-source beamforming measurements.

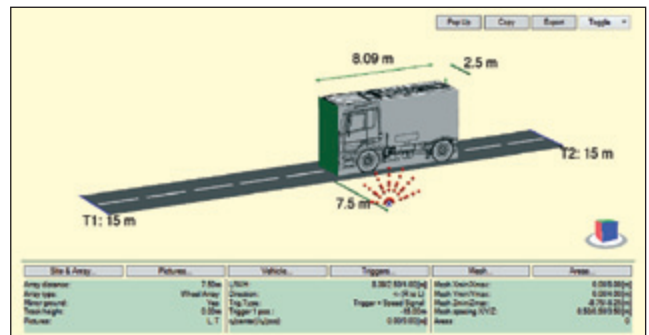


Figure 9. Geometry setup for defining relevant measurement site, array, trigger, mesh and vehicle layout parameters.

was used. Using a sampling frequency of 8192 Hz and a recording time of 9.249 seconds, a total of 75776 samples were recorded in each measurement channel.

Figure 9 shows how most relevant parameters can be entered with a visual feedback of the test site layout. Here we define six individual parameters such as array type and distance from the track. Pictures or drawings from five sides of the vehicle can be inserted – to be overlaid with measurement results, vehicle dimensions, photo cell (trigger) and radar/GPS (speed) settings, mesh dimensions for the noise maps and area definitions for sound power calculation and source ranking.

Before any calculation is initiated and to obtain a quick overview, a graph display shows vehicle position vs. time (Figure 10a) and a second (10b) shows pass-by A-weighted sound pressure level from the array microphone which has the closest location to the ISO 362 measurement point.

In this measurement case, the result is from array microphone

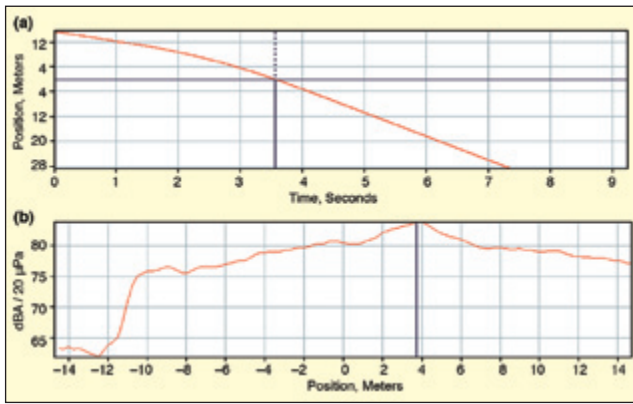


Figure 10. (a) Plot shows vehicle position vs. time; (b) A-weighted SPL at microphone position No. 22 (ISO 362 point).

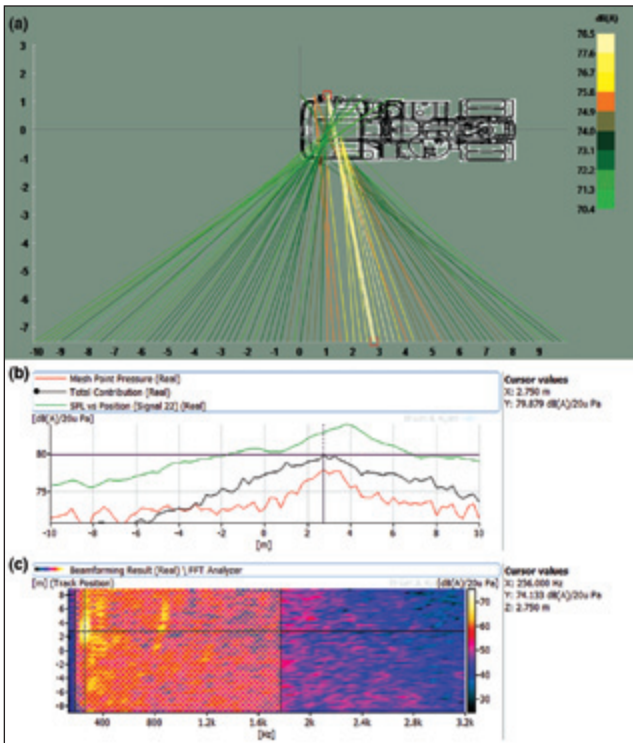


Figure 11. Preview of data for validation of the beamforming results: (a) Line diagram; (b) SPL curves; and (c) SPL contour plot.

No. 22. The upper graph shows that the front of the truck has reached the 0-m track location after 3.56 s, and the lower graph shows that a maximum of 83.9 dBA is found when the front of the truck is at location 3.75 m on the test track.

The complete calculation setup is very simple even for the occasional user:

- Select frequency range, constant (FFT) or constant percentage bandwidth resolution (1/1, 1/3 or 1/12 octaves), frequency weighting (A, C or Lin).
- Select start, stop and interval positions, e.g. from -10 m to +10 m with intervals of 25 cm.
- There are two parameters dedicated for moving source applications, namely the use of shading (outdoor) for handling air turbulence and use of upsampling (factor of 16) of time signals to improve accuracy.

After the calculation is initiated, the first preview results are available for validation purposes. There are three graphs linking mesh points, vehicle position, frequency and sound levels on array location. The lower graph (Figure 11c) is a short-time Fourier transform plot of the vehicle “max level mesh point” (explained later) sound pressure level contribution at the array center based on beamforming calculations shown as track position vs. frequency. In this contour plot, we can see some higher levels in the frequency interval between 200 and 1700 Hz, which is highlighted using a

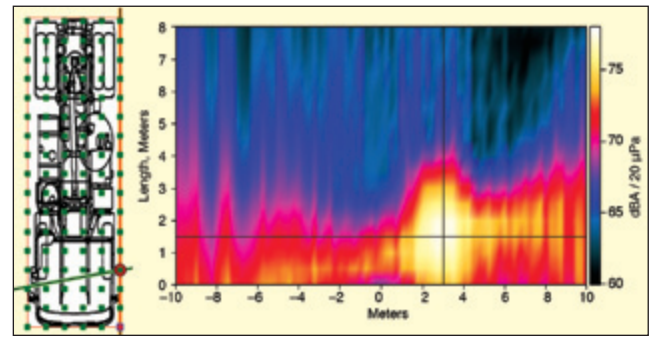


Figure 12. Sound pressure level contour plot using local spatial coordinates (vehicle mesh point direction) vs. global spatial coordinates (track position); at left is indication of sound emission direction for contour plot cursor location from top of vehicle.

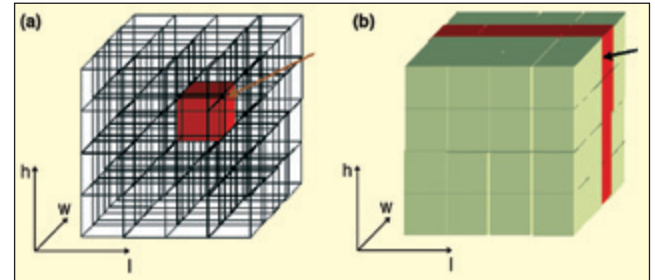


Figure 13. (a) Selected volume for beamforming mapping; (b) Selected plane for beamforming mapping.

delta cursor. On the position axis, we can see that the highest level occurs around position 2.75 m. A-weighting can be toggled on or off, but all the plots in this article are shown with A-weighting.

The middle graph (Figure 11b) shows three curves, where the upper curve is a duplicate of the measured SPL at microphone position 22 closest to the ISO 362 point, (similar to Figure 10b) and is shown here for further validation purposes.

The lower curve in Figure 11b is extracted from the beamforming-based contour plot in Figure 11c and is also directly related to the upper graph (line diagram in Figure 11a). Thus, it shows the “max level mesh point” sound pressure level at the array center calculated at each position interval (25 cm) from the frequency interval indicated by the delta cursor in the contour plot. The middle curve in Figure 11b is the total contribution of the whole vehicle as a function of vehicle position in the above-mentioned frequency band.

Figure 11a indicates the different “max level mesh point” for each track interval length along the X axis for the selected frequency range. So this line diagram axis is distance vs. track position. The color-coded lines indicate level, and the lines link the track position on the x-axis to the mesh point of the vehicle responsible for that maximum pressure contribution. As seen, the area around the right front wheel gives the highest contribution when the front of the truck is at track position 2.75 m.

An additional view of the beamforming data closely related to the line diagram in Figure 11a is shown in Figure 12. Again the maximum levels are found in the direction at mesh point 1.5 m (y-cursor location) on the vehicle, which is around the front wheels and observed at track position 3 m (x-cursor location).

When verifying from the preview that all calculation parameters are correctly chosen and adjusted, a final calculation may be performed and the results stored in the database.

For beamforming source location mapping, a 3D mesh is defined, meaning that any point (volume), line or plane can be mapped within this definition (see Figure 13). This is extremely useful when measuring on an open truck, as shown in Figure 8. In most other cases, it is only relevant to make mapping on the surface of the defined mesh, which corresponds to mapping of the sound field on the surface of the vehicle.

Noise source mapping is a well-known application, which for nonstationary sound sources also includes animation of maps as a function of time, position, rpm, shaft angle, etc. Only one example

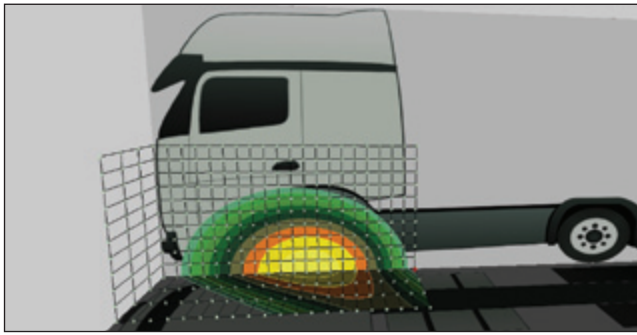


Figure 14. Noise source mapping with choice of multiple planes from road vehicle moving-source beamforming test.

is shown in this article (Figure 14). The example is from a non-stationary analysis and shows the pressure contribution (at array center position) at a vehicle location 3 meters in the frequency interval from 100 Hz to 500 Hz, where the major sound sources are located around the front wheels.

### Measurements on Rail Vehicles

A measurement campaign was done to investigate the rolling noise of regional trains along the line of the north-south coastal route from Copenhagen to Helsingør, Denmark. The sound power of the individual bogies was determined by means of MSB measurements using a 2.5-m diameter planar array (Figure 15).

Each of the nine arms, had six microphones spaced logarithmically from the center of the array. All microphones were fitted with wind shields. To measure the speed of the train (assumed to be constant for the duration of the passage through the measurement zone), trigger pulses were employed from two photocells, placed some 43 m apart (Figure 16).

A visible laser was used to align the triggers and measure the distances from the array to the rails. The trigger pulses were of different duration so the direction of travel of the trains could be determined and stored with the acoustical data.

After installing the array and two photocells, which took less than an hour, MSB recordings were made for all the trains that passed by in the following two hours. All recordings were stored in a database with details of the trains that were composed of either three or six carriages. The speeds varied from 114 to 125 km/hr. Permission to perform the measurements was obtained in advance from the railway authorities, but no special safety regulations or security personnel were required, since all measurement activities took place outside the boundary of the railway property. Also for these measurements, a shading filter (area weighting) was applied to the microphone signals so that only the central part of the array is used at high frequencies.

The spatial resolution of the DAS maps was further improved by applying deconvolution; in this case, the non-negative, least-squares (NNLS) algorithm is used. The output of the deconvolution is basically the strength of the monopoles allocated in frequency bands and distributed spatially (see Figure 17). Finally, on the sound intensity contour maps of the six trains in the measurement campaign, the sound power from around the various bogies was determined within some predefined areas.<sup>7,11</sup>

### Blade Tracking on Wind Turbines

Noise problems can appear a long time after a turbine has been installed; for example, a crack could appear on one of the blades. In such cases, the operator of the turbine may not be able to easily localize the position/cause of the noise, which might introduce lengthy troubleshooting to make visual inspection of the blades. In these cases, beamforming can also be a useful tool, since it can localize the position of the dominant sources.

Knowing the position of the turbine and measuring the blade's azimuth angle, the focus points can follow the movement of the blades, and the noise map can be visualized on the blade for each azimuth angle step. The array used for the following measurement has an elliptical shape (13.6 m × 8.5 m) as illustrated in Figure 18. It consists of nine lines of microphones lying on the ground (flush



Figure 15. Logarithmic wheel array with 56 microphones and nine arms used for measurements on trains.

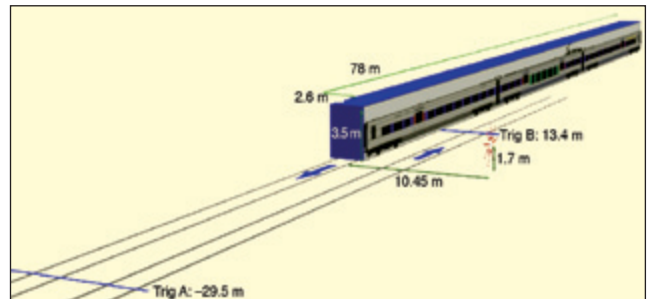


Figure 16. Interactive site setup with positions of tracks, photocells and array to document measurements.

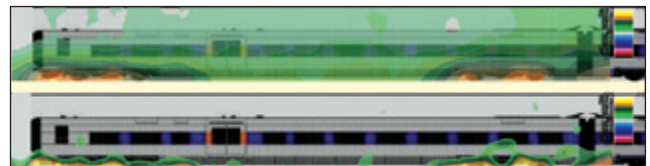


Figure 17. Train moving at 114 km/hr to left; sound intensity contours with same scale mapped on surface of train; frequency range 160-6368 Hz (top - DAS; bottom - NNLS deconvolution).

mounted in rigid plates) with 12 microphones per line.

In this example, the measurement is performed on a wind turbine with a rotor diameter of 100 metres, and deconvolution may be applied in conjunction with the tracking beamforming to improve the spatial resolution in the final results. The array must not be too close to the turbine, since a small difference in angle seen from the array corresponds to a large distance on the rotor surface. Conversely, since the beamformer's resolution is inversely proportional to the measurement distance, the array must not be too far away either. A good compromise between these two issues is to place the array so that the nacelle is at 45° from the ground seen from the array. This is why the array was positioned at 100 m from the tower (see Figure 19).

Beamforming can be processed with or without tracking the

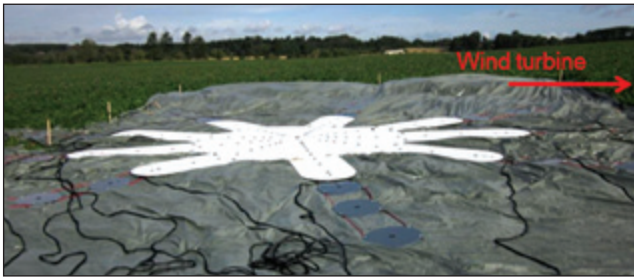


Figure 18. Ground array seen from side; right-hand side points toward wind turbine.

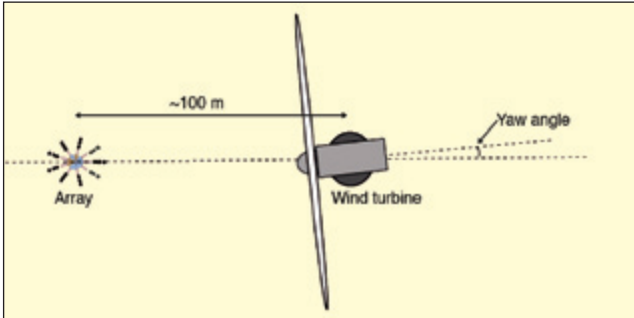


Figure 19. Array located in front of wind turbine; yaw angle defined as  $0^\circ$  when nacelle points toward array, and this angle increases as nacelle rotates counterclockwise.

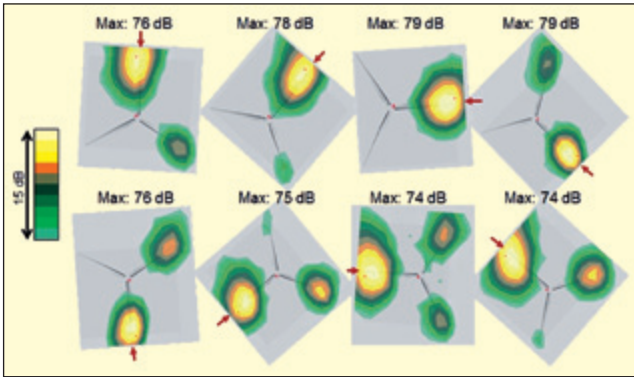


Figure 20. DAS beamforming with blade tracking at 1 kHz (1/3-octave band); plots show estimated sound pressure level on rotor surface as a function of blade positions (which rotate clockwise); red arrows indicate position of Blade 1 on each plot, indicating maximum level of map (nacelle yaw =  $3^\circ$ ).

position of the blades. If the blade positions are not measured, the focus points are stationary in space, and the beamformer will give an average value over a small time interval for each focus point. The disadvantage is that the result is smeared when the source passes through several reconstruction points in the time intervals; the faster the source is moving, the more smeared the result will be. The optimal results of the beamformer can be achieved if the 3D positions of the blades are known as a function of time. Such a tracking, moving-source beamforming approach makes it possible to average over the time interval without smeared results, because the focus point follows the position of the source.

Figure 20 shows the results of a tracking DAS calculation measurement with the nacelle at a yaw angle of  $3^\circ$ . Contributions from the tip of the blades dominate as expected due to the higher speed at the end of the blade and the turbulences around it. Inaccuracies in measuring the position and orientation of the nacelle could have significant consequences on the maps, but the hot spots are seen to follow the tips well for all angles (shown with  $45^\circ$  interval steps indicated by the red arrow), which shows that the tracking works as intended. One of the blades is the dominant contributor at all azimuth angles. As expected, this is Blade 1 due to the noise from a loose wire and mounting of three accelerometers, which were used for other purposes than array measurements. During downward movement, noise from the other blades is also visible on the map, but the strongest source is still Blade 1 even when it

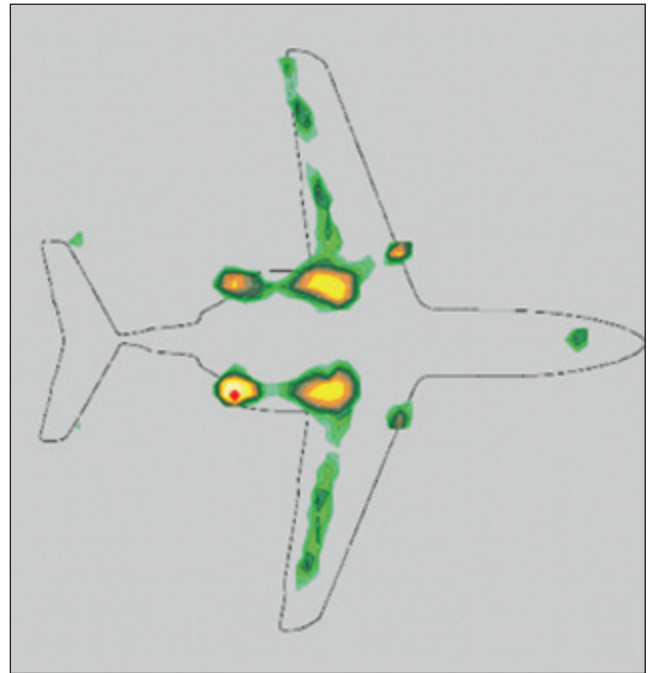


Figure 21. Sound intensity data at 2 kHz from level flight with engine idle and aircraft in landing configuration; display dynamic range is 20 dB corresponding to 2 dB contour interval.



Figure 22. Array on runway is 12 meters in diameter with nine radial arrays, each with 12 microphones (108 total).

approaches  $0^\circ$  (blade points upward).<sup>12</sup>

### Fly-over Beamforming

Examples of fly-over beamforming are found in References 6, 10 and 13. Figure 21 shows the results at the 2 kHz, one-third-octave band of a fly-over measurement on an MU300 business jet. Its overall length and width are 14.8 and 13.3 meters, respectively. It has two jet engines on the body, just behind and over the wings. The array measurements were taken with the airplane flying over the runway at an altitude of approximately 60 meters and speed of about 60 m/s ( $\approx 220$  km/h).


The 12-meter diameter spoke wheel microphone array consisted of 108 microphones ( $9 \times 12$ ), as shown in Figure 22. The major sources are engine intake and exhaust as well landing gear and the wing flaps. The calculation requires the use of tracking, shading, Doppler correction, cross-spectrum matrix main-diagonal (auto-spectra) removal and de-convolution beamforming techniques.

### Conclusions

This article describes a practical microphone array system designed for noise source identification on moving sound sources. The theory of beamforming methods is given with a description of shading methods for handling the loss of coherence, for example, due to air turbulence, as we might experience when using large

outdoor arrays. Finally, some analysis results from moving source beamforming measurements are presented.

## References

1. J. Hald and J. J. Christensen, "A Novel Beamformer Design for Noise Source Location from Intermediate Measurement Distances," *Proceedings of ASA/IFA/MIA*, 2002.
2. J. J. Christensen and J. Hald, "Beamforming," Brüel & Kjær Technical Review No. 1, pp. 1-48, 2004.
3. J. Hald, "Combined NAH and Beamforming Using the Same Array – SONAH," Brüel & Kjær Technical Review No. 1, pp. 11-50, 2005.
4. Klaus Ehrenfried and Lars Koop, "A Comparison of Iterative Deconvolution Algorithms for the Mapping of Acoustic Sources," American Institute of Aeronautics and Astronautics, *AIAA Journal*, Vol. 45, No. 7, pp. 1584-1595, 2007.
5. Bernard Ginn and Jørgen Hald "Aerodynamic Noise Source Identification In Wind Tunnels Using Acoustical Array Techniques," Eighth MIRA International Vehicle Aerodynamics Conference – Low Carbon Vehicles, 2010.
6. Jørgen Hald, Yukata Ishii (B&K) and Ishii, Oinuma, Nagai, Yokogawa, Yamamoto (JAXA), "High-resolution Fly-over Beamforming Using a Small Practical Array," American Institute of Aeronautics and Astronautics, *AIAA Journal* (2012) and Brüel & Kjær Technical Review No. 1, BV 0064-11, 2012.
7. Jesper Gomes, Jørgen Hald and Bernard Ginn, "Localising Noise Sources on a Rail Vehicle During Passby," International Workshop on Railway Noise, 2013.
8. P. Sijtsma, and R. Stoker, "Determination of Absolute Contributions of Aircraft Noise Components Using Flyover Array Measurements," AIAA Paper 2004-2958, 2004.
9. S. Gade, J. Hald, B. Ginn, "Noise Source Identification with Increased Spatial Resolution Used in the Automotive Industry," JSAE paper No. 20125015, 2012.
10. S. Gade, J. Hald, B. Ginn, "Noise Source Identification with Increased Spatial Resolution," *Sound & Vibration*, April 2013, pp 9-13, 2013.
11. B. Ginn, J. Gomes, and J. Hald, "Recent advances in Rail Vehicle Moving Source Beamforming," Proceedings of Inter-Noise 2013.
12. J. Gomes, "Noise Source Identification with Blade Tracking on a Wind Turbine," Proc. Inter-Noise, 2012.
13. Jørgen Hald, "High-Resolution Flyover Beamforming Using a Practical Array," Proceedings of Berlin Beamforming Conference 2014. 

The author can be reached at: [svend.gade@bksv.com](mailto:svend.gade@bksv.com).